Wang, *Astrophys. J.* **435**, L153 (1994).
18. J. T. Gosling *et al.*, *J. Geophys. Res.* **77**, 5442 (1972).
19. J. L. Phillips *et al.*, *Geophys. Res. Lett.* **19**, 1239 (1992).
20. We thank our colleagues at Sandia National Laboratories and Los Alamos National Laboratory (LANL) for their contributions to the solar wind plasma experiment, R. K. Sakurai and S. J. Kedge for data reduction support, A. Balogh for the magnetometer observations used in Fig. 6, J. T. Hoeksema for Wilcox Solar Observatory magnetic field observations and calculations, and R. J. Forsyth and N. R. Sheeley Jr. for helpful discussions. The support of the Ulysses Project Offices and project scientists at Jet Propulsion Laboratory (JPL) and European Space Technology Center is gratefully acknowledged. Work at LANL was carried out under the auspices of the U.S. Department of Energy with National Aeronautics and Space Administration (NASA) support. Work at JPL of the California Institute of Technology was performed under contract to NASA.

31 January 1995; accepted 18 April 1995

The Southern High-Speed Stream: Results from the SWICS Instrument on Ulysses

J. Geiss, G. Gloeckler, R. von Steiger, H. Balsiger, L. A. Fisk, A. B. Galvin, F. M. Ipavich, S. Livi, J. F. McKenzie, K. W. Ogilvie, B. Wilken

The high-speed solar wind streaming from the southern coronal hole was remarkably uniform and steady and was confined by a sharp boundary that extended to the corona and chromosphere. Charge state measurements indicate that the electron temperature in this coronal hole reached a maximum of about 1.5 million kelvin within 3 solar radii of the sun. This result, combined with the observed lack of depletion of heavy elements, suggests that an additional source of momentum is required to accelerate the polar wind.

A principal aim of the Ulysses mission was to investigate directly the solar wind coming out of the polar coronal holes. These low-temperature regions of the corona were known to emit high-speed streams (HSSTs), and it was hoped that a dynamically steady and geometrically simple outflow from the corona would be found that would lend itself more readily to theoretical interpretation than the unsteady and geometrically complex solar wind patterns encountered at lower heliographic latitudes. The task was facilitated by the fact that Ulysses is passing over the poles of the sun during the quiet years of the solar cycle, when the coronal holes are largest: The spacecraft collected data for more than a year from an HSST that covered a solid angle of nearly 60% of the southern hemisphere.

We present here results from the Solar Wind Ion Composition Spectrometer (SWICS) on board Ulysses (*1*). For each ion, the instrument measures energy per charge with an electrostatic analyzer and determines—after an acceleration by 23 kV—the time-of-flight and the total energy with solid-state detectors. With this technique, the mass M and charge q are determined separately, so that different ion species can be distinguished even if they have identical M/q ratios. Thus, ion pairs such as C^{6+} and He^{2+}, Mg^{10+} and C^{5+}, or Mg^{8+} and C^{4+} can be separated. This separation allowed measurement of the chemical abundances of C and Mg in the solar wind and ion charge spectra of several elements. Both of these capabilities are important for studying processes in the solar wind source region, that is, the place in the chromosphere and corona from where the solar wind flow originates.

During its voyage to Jupiter, Ulysses detected the typical solar wind, which is quite variable (Fig. 1). Only a few months after the spacecraft left the ecliptic plane, it began to encounter an extension of the HSST emitted by the southern coronal hole. The HSSTs are characterized by high speeds (V > 600 km/s) and low freeze-in temperatures (*2*). From about July 1992 to about May 1993, the spacecraft regularly went into and out of the HSST every solar rotation, and since it has been continuously engulfed in the HSST. The solar wind parameters were much more uniform in the HSST than in the solar wind at lower latitude, and therefore, averages of flow parameters and abundance ratios inside the HSST are an adequate basis for theoretical interpretation.

Differences between abundances in the solar wind and its source reservoir, the outer convective zone of the sun, are created in the chromosphere and the corona. An ion-atom separation mechanism operating at the temperatures prevailing in the chromosphere produces a systematic overabundance of elements with low first-ionization potential (the FIP effect) (*3*). In the corona, a changing efficiency of momentum transfer among the ions or from fields and waves to ions causes variations in solar wind composition (*4, 5*).

In Fig. 2, the relative abundances of nine elements in the slow solar wind and in the southern HSST are plotted as a function of ionization time calculated for solar surface conditions (*6*). A systematic abundance relation is observed, indicating that a competition between the ionization time and a characteristic time for ion-atom separation underlies the FIP effect (*7*). There is a systematic difference between the abundances in the slow solar wind and the HSST: The FIP effect is definitely reduced in the latter (*6, 8*), implying different chromospheric structure or processes below coronal holes.

From mid-1992 to the spring of 1993, Ulysses went into and out of the southern

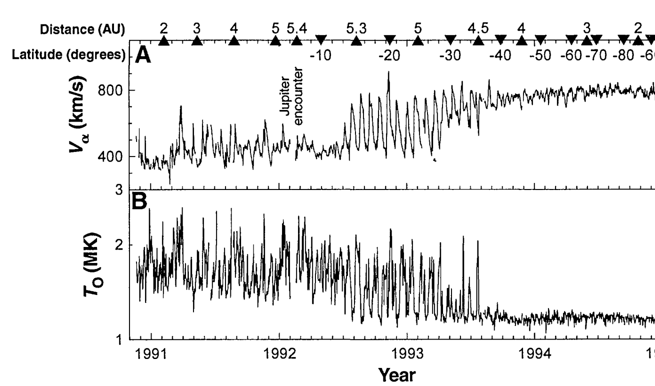

Fig. 1. The changing solar wind conditions encountered by Ulysses during 4 years of observation. (**A**) The speed of the He ions, V_α, and (**B**) the freeze-in temperature (*2*) of O, T_O, as a function of time and the heliographic latitude of Ulysses (distance from the sun in astronomical units is also given). The varying conditions at lower latitude contrast with the quiet flow at higher latitude. During 10 months in 1992 and 1993, the spacecraft regularly went into and out of the HSST from the southern polar coronal hole. The HSSTs are identified by the combination of high velocity and low freeze-in temperatures.

J. Geiss, Physikalisches Institut, University of Bern, 3012 Bern, Switzerland, and Department of Atmospheric, Oceanic and Space Sciences, University of Michigan, Ann Arbor, MI 48109, USA.
G. Gloeckler, A. B. Galvin, F. M. Ipavich, Department of Physics, University of Maryland, College Park, MD 20742, USA.
R. von Steiger and H. Balsiger, Physikalisches Institut, University of Bern, 3012 Bern, Switzerland.
L. A. Fisk, Department of Atmospheric, Oceanic and Space Sciences, University of Michigan, Ann Arbor, MI 48109, USA.
S. Livi, J. F. McKenzie, B. Wilken, Max-Planck-Institut für Aeronomie, D-37189 Katlenburg-Lindau, Germany.
K. W. Ogilvie, National Aeronautics and Space Administration, Goddard Space Flight Center, Greenbelt, MD 20771, USA.

HSST every solar rotation (Fig. 1). Using the data of this period, we studied the systematics in the variations of solar wind properties across the border between the slow solar wind and the HSST by means of a superposed epoch method (9). The freeze-in temperatures of C and O (T_C and T_O) and the Mg/O and Fe/O ratios followed each other very closely, and the transition between low and high values of these physical parameters was very steep (Fig. 3). Statistical analyses show that it is as steep as a step function would be if subjected to our procedure. Thus, the chromosphere and the corona have a common, relatively sharp boundary, separating the low-FIP from the high-FIP region in the chromosphere and the low-temperature from the high-temperature region in the corona (9). The existence of such a common boundary points to a causal relation of the kind for which conditions in or even below the chromosphere determine the supply of energy into the corona. Thus, discussions of the origin of the solar wind should include chromospheric as well as coronal processes.

The speed of the solar wind declined slowly at the trailing edge of the HSST (Fig. 3), as it was observed in the ecliptic plane during the solar minimum in the mid-1970s (10). Mapping the solar wind back to the corona shows that the large range of decreasing velocities comes from a relatively restricted range in longitude (11). This implies that the boundary between low and high values of T_O, T_C, Mg/O, and Fe/O at the eastern rim of the coronal hole is even sharper than is indicated in Fig. 3. On the other hand, as a result of solar rotation, the HSST rams into the slow wind at its western rim, causing shocks and other kinetic and thermal perturbations (12), but as expected, the chromospheric and coronal ionic markers of the boundary between the two wind types remain well defined.

Ultraviolet investigations of coronal holes with Orbiting Solar Observatory 4 (OSO-4) (13) and Skylab (14) showed that the emission of Mg X (representing a temperature of 1.6 MK) changed steeply (within less than 10 arc sec) at the coronal hole boundary. Although the boundary is less well defined for the Ne VIII and Ne VII lines (representing 0.8 to 0.5 MK), the emissions of these ions changed simultaneously with that of Mg X. These ultraviolet observations show that coronal holes have well-defined and steep boundaries, which agrees with our results derived from the freeze-in temperatures in the solar wind.

The Skylab data showed that the transition zone is thicker below coronal holes (14). The reduction in the strength of the FIP effect reported here (compare Mg/O and Fe/O in Fig. 3) demonstrates that the sharp change in the characteristics of the solar atmosphere continues farther down into the chromosphere and probably has its source in the outer convective zone.

The sharp temperature step at the rim of the coronal hole and the similarly sharp step in the freeze-in temperature at the rim of the HSST demonstrate that both define the same boundary at two different solar distances, allowing a derivation of the degree to which the expansion in the coronal hole is superradial (9). Furthermore, this identification of the boundary of the coronal hole far away from the sun shows that the slow solar wind does originate outside of the coronal hole.

Ion abundances were remarkably steady inside the southern HSST. For instance, no systematic latitudinal variation in T_O above the noise is discernible in Fig. 1. On the other hand, a small increase in the velocity of He ions V_α with increasing solar latitude is indicated (Fig. 1).

The distribution of the charge states ("charge spectra") for all heavy elements (atomic number $Z > 2$) was different in the southern HSST compared to the slow solar wind, reflecting the lower temperature in coronal holes (14). These charge spectra are valuable indicators of coronal temperature

Table 1. Relative abundance of the most abundant ions of C, O, Si, and Fe observed with SWICS in the HSST, the corresponding freeze-in temperatures, and the electron ionization and recombination coefficients at these temperatures.

Ion pair	Abundance ratio	Freeze-in temperature (MK)	Ionization coefficient (k_I) (10^{-12} cm^3/s)	Recombination coefficient (k_R) (10^{-12} cm^3/s)
C^{6+}/C^{5+}	0.20	0.96	0.24	1.19
C^{5+}/C^{4+}	2.40	1.03	3.09	1.28
O^{7+}/O^{6+}	0.033	1.17	0.05	1.58
Si^{10+}/Si^{9+}	0.52	1.43	17.3	33.6
Si^{9+}/Si^{8+}	1.43	1.34	40.0	27.8
Fe^{12+}/Fe^{11+}	0.64	1.28	67.2	105.4
Fe^{11+}/Fe^{10+}	0.92	1.20	95.5	104.2
Fe^{10+}/Fe^{9+}	1.71	1.26	191.7	112.5

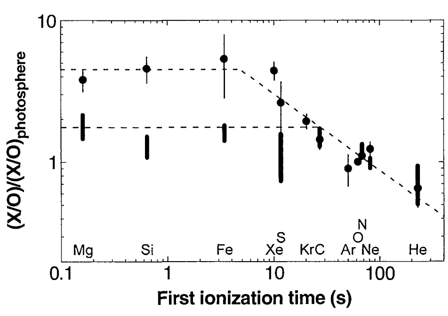

Fig. 2. Element abundances relative to O in the slow solar wind (circles) and in the southern HSST (bars) (6). The abundances are normalized to the photospheric abundances and plotted as a function of ionization time, assuming inferred solar surface conditions (7).

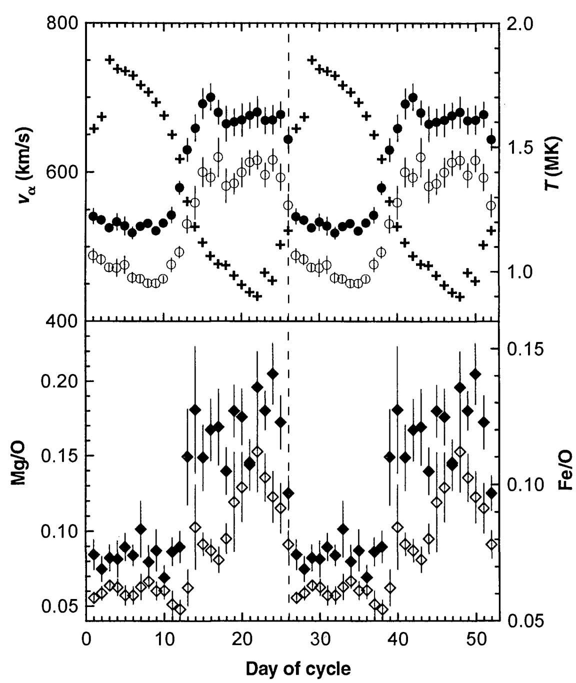

Fig. 3. Superposed epoch plot of SWICS data from day 191 of 1992 to day 98 of 1993 (22), when Ulysses went regularly into and out of the HSST once every solar rotation (26-day average duration) (Fig. 1). The method (9) is based on the 600 km/s crossings of the He speed. The speed of He ions V_α (+), the coronal freeze-in temperatures of O (●) and C (○), and the abundance ratios Mg/O (◆) and Fe/O (◇) are shown (23). The data are repeated after the dotted line to facilitate the recognition of the entire pattern. The steep changes in the freeze-in temperatures and abundance ratios demonstrate a sharp boundary of the HSST that reaches down into the corona and chromosphere.

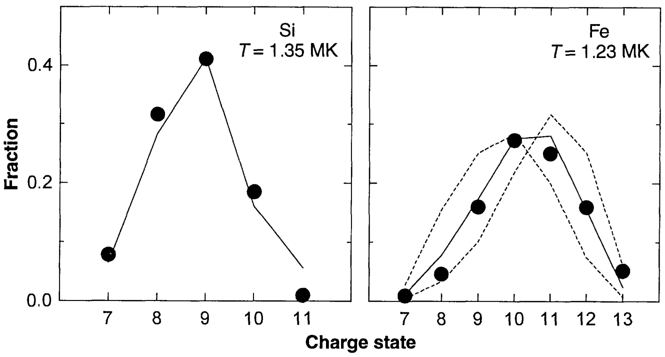

Fig. 4. The charge spectra of Si and Fe observed in the HSST (dots) compared with equilibrium freeze-in distributions (lines) for temperatures of 1.35 and 1.23 MK, respectively. In the case of Fe, the distributions are also given for 1.13 and 1.33 MK (dashed lines). This shows that major contributions of ions with 0.1 MK higher or lower freeze-in temperature would result in a broadening of the charge spectra that is not observed, constraining temperature variations at freeze-in altitudes even at very fine lateral scale.

conditions (*15*). An estimate of the temperatures and temperature gradients in the coronal source region can be obtained from the equilibrium freeze-in temperatures (*2, 15*). For a quantitative interpretation of charge spectra, the gradual freezing-in has to be calculated by dynamical solar wind expansion models (*16*).

As expected from model calculations (*16*), a considerable range in freeze-in temperatures was found (Table 1), but for ion pairs of the same element, the differences are small. In fact, a single freeze-in temperature gives a good representation for the abundances of the major ions of a given element (Fig. 4). The narrowness of the charge spectra in Fig. 4 implies that temperatures at the freeze-in altitudes are homogenous, down to the smallest lateral scale (*17*).

The differences between T_C, T_O, T_{Si}, and T_{Fe} allow us to draw some conclusions concerning the vertical temperature structure in the corona (Fig. 5). The electron density n_e at which the freezing-in of an ion pair occurs is proportional to $(k_I + k_R)^{-1/2}$, where k_I and k_R are the corresponding ionization and recombination coefficients (*15*). Thus, for n_e decreasing with altitude, we expect C and O to freeze-in closest to the sun, followed by Si and then Fe. In the region of decreasing temperature, ionization rates drop rapidly and the final adjustments in the charge spectra are mainly by recombination, that is, freeze-in altitudes are here determined by the recombination coefficients k_R. Because k_R(Fe) is larger than k_R(Si), our observation of $T_{Si} > T_{Fe}$ implies that the Fe charge states froze-in at an altitude above the temperature maximum. On the other hand, both T_C and T_O are less than T_{Si} and T_{Fe}, and because the rate coefficients of C and O are much smaller than those of Si and Fe (Table 1), the charge states of C and O must have frozen before the expanding plasma even reached the temperature maximum. Thus, with the charge state observations of C, O, Si, and Fe, we bracket the altitude of the temperature maximum, as expected from the coronal hole expansion model (*16*). The temperature maximum occurs at 1.5 solar radii from the center of the sun in that model, but this depends on the adopted electron density (Fig. 5).

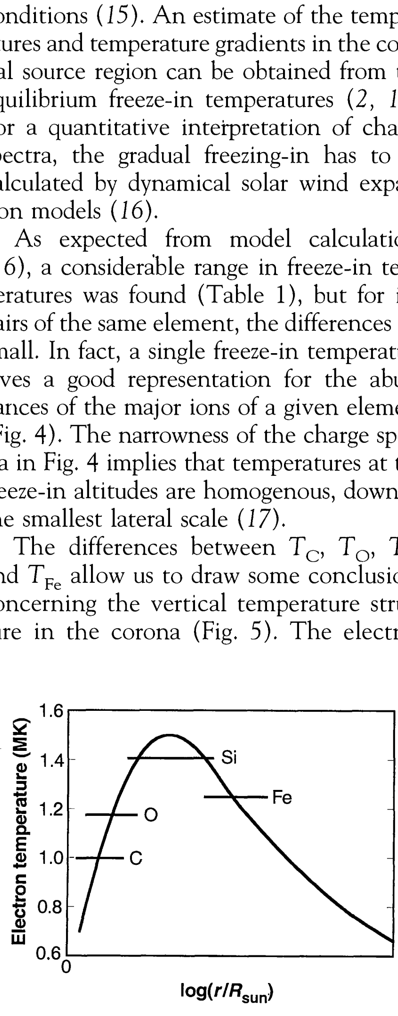

Fig. 5. Sketch of the freezing-in situation in the southern coronal hole. We do not wish to give an absolute scale on the abscissa before modeling is done with the electron densities that prevailed in the southern coronal hole while Ulysses flew over it. The SWICS data imply that the charges of C and O never came close to the equilibrium distribution corresponding to the electron temperature maximum, and in this sense C and O "froze-in below this maximum." On the other hand, the data indicate that the charges of Fe remained approximately in equilibrium with the electron temperature up to its maximum and then froze in the declining temperature regime.

Our observations imply that the heat content in the southern coronal hole was not sufficient to account for the energy in the HSST. (i) Aside from the reduced FIP effect, which has its cause in the upper chromosphere, we do not detect a depletion of heavy elements in the HSST. The density of protons in the coronal hole, however, is insufficient to accelerate the heavy species by Coulomb drag (*16*). (ii) The charge spectra of C, O, Si, and Fe bracket the position of the electron temperature maximum. Combining observed densities in coronal holes with the k_I and k_R values in Table 1, we estimate the maximum temperature to occur below an altitude of 3 solar radii with a peak electron temperature not much exceeding 1.5 MK (*18*). Unless the proton temperature at these altitudes is very much higher, the heat content in the corona does not account for the energy carried away by the HSST, even if ample allowance is made for heat conduction. These observations imply that an additional supply of momentum is required (*19*).

REFERENCES AND NOTES

1. G. Gloeckler *et al.*, *Astron. Astrophys. Suppl. Ser.* **92**, 267 (1992).
2. A freeze-in temperature is calculated from a pair of ions under the assumption of local equilibrium between electron impact ionization and recombination. In our notation, T_E is the freeze-in temperature calculated from the most abundant ions of the element E. For instance, T_O and T_C are the freeze-in temperatures derived from O^{7+}/O^{6+} and C^{6+}/C^{5+}, respectively. Because ionization rate constants are strongly temperature dependent, freeze-in temperatures give information about electron temperatures in the corona.
3. See J. P. Meyer, *Adv. Space Res.* **13**, 377 (1993).
4. J. V. Hollweg, *J. Geophys. Res. A* **86**, 8899 (1981).
5. A. Bürgi and J. Geiss, *Solar Phys.* **103**, 347 (1986).
6. We have used in this some new data as well as published data obtained with various instruments on different spacecraft. For references on original data, see G. Gloeckler and J. Geiss, *AIP Conf. Proc.* **183**, 49 (1989); P. Bochsler, in *Solar Wind Seven*, E. Marsch and R. Schwenn, Ed., vol. 3 of the *COSPAR Colloquia Series* (Pergamon, New York, 1992), p. 323; J. Geiss, G. Gloeckler, R. von Steiger, *Philos. Trans. R. Soc. London Ser. A* **349**, 213 (1994). Abundances of Kr and Xe were derived from particles trapped at the lunar surface by R. Wieler, H. Baur, and P. Signer [*Lunar Planet. Sci.* **XXIV**, 1519 (1993)].
7. J. Geiss and P. Bochsler, in *Rapports Isotopiques dans le Systeme Solaire* (Cepadues-Editions, Paris, 1985), p. 213; in *The Sun and Heliosphere in Three Dimensions*, R. G. Marsden, Ed. (Reidel, Dordrecht, Netherlands, 1986), pp. 173–186; R. von Steiger and J. Geiss, *Astron. Astrophys.* **225**, 222 (1989).
8. The reduced FIP strength in HSSTs was first detected by the Active Magnetospheric Particle Tracer Explorer (AMPTE) spacecraft in the heated solar wind plasma of the magnetosheath [G. Gloeckler, F. M. Ipavich, D. C. Hamilton, B. Wilken, G. Kremser, *Eos* **70**, 424 (1989); R. von Steiger, S. P. Christon, G. Gloeckler, F. M. Ipavich, *Astrophys. J.* **389**, 791 (1992)].
9. J. Geiss, G. Gloeckler, R. von Steiger, *Space Sci. Rev.* **72**, 49 (1995).
10. J. S. Bame, J. R. Asbridge, W. C. Feldman, J. T. Gosling, *J. Geophys. Res.* **82**, 1487 (1977).
11. J. T. Nolte, A. S. Krieger, E. C. Roelof, R. E. Gold, *Solar Phys.* **51**, 459 (1977).
12. The forward and reverse shocks of these corotating interaction regions (CIRs) are discernible in Fig. 3. The CIRs have been the subject of many publications, for example, J. T. Gosling *et al.*, *Space Sci. Rev.* **72**, 99 (1995).
13. G. L. Withbroe *et al.*, *Solar Phys.* **21**, 271 (1971).
14. R. Tousey *et al.*, *ibid.* **33**, 265 (1973); M. C. E. Huber *et al.*, *Astrophys. J.* **194**, L115 (1974).
15. A. J. Hundhausen, H. E. Gilbert, S. J. Bame, *J. Geophys. Res.* **73**, 5485 (1968); S. P. Owocki, T. E. Holzer, A. J. Hundhausen, *Astrophys. J.* **275**, 354 (1983).
16. The HSST composition data can be compared with the results from model 5 of Bürgi and Geiss (*5*). It is an expansion model based on observed densities in coronal holes that takes into account the finite abundance of He, different speeds for different elements, superradial expansion geometry, and direct momentum transfer from waves. The predictions of model 5 for the charge state spectra of C and O agree quite well with the SWICS observations in the southern HSST. For Si, Bürgi and Geiss used recombination and ionization coefficients (*20*) that have since been revised . With the new coefficients (*21*), predicted and observed charge state spectra are also in reasonable agreement for Si.

17. P. Bochsler [in *Solar Wind Five*, M. Neugebauer, Ed., *NASA CP-2280* (1983), p. 613] has discussed the broadening of charge state spectra resulting from mixing ion populations originating at different temperature.
18. Freeze-in temperatures are calculated here by assuming Maxwellian distribution functions for the electrons. Distorted distribution functions (κ distributions) would lead to even lower freeze-in temperatures [A. Bürgi, *J. Geophys. Res. A* **92**, 1057 (1987)].
19. Theoretical studies and modeling have lead many authors to discuss plasma waves as an important momentum source for driving HSSTs; see R. H. Munro and B. V. Jackson, *Astrophys. J.* **213**, 874 (1977); J. V. Hollweg, *Rev. Geophys.* **16**, 689 (1978); *J. Geophys. Res.* **91**, 4111 (1986); J. F. McKenzie, W.-H. Ip, W. I. Axford, *Astrophys. Space Sci.* **64**, 183 (1979); R. Lallement, T. E. Holzer, R. H. Munro, *J. Geophys. Res.* **91**, 6751 (1986); (*15*).
20. J. M. Shull and M. Van Steenberg, *Astrophys. J. Suppl. Ser.* **48**, 95 (1982).
21. M. Arnaud and R. Rothenflug, *Astron. Astrophys.* **60**, 425 (1985); M. Arnaud and J. Raymond, *Astrophys. J.* **398**, 394 (1992).
22. One solar rotation (days 308 through 334 of 1992) was omitted because a coronal mass ejection occurred, so that our analysis includes 9.5 solar rotations.
23. The data for V_α and T_O are the same as those shown earlier (*9*), whereas that for T_C and Fe/O are new. For Mg/O, we used the charge spectrum Mg^{6+} to Mg^{10+} for determining the Mg abundance, which should reduce systematic errors, as compared to our earlier publication (*9*), where we used the main ion Mg^{10+} and estimated the abundances of the other Mg ions by assuming identical freeze-in temperatures for Mg and O.
24. We are very grateful to the teams of engineers and physicists in our institutions as well as the project teams of the European Space Technology Center and the European Space Operations Center of the European Space Agency and the Jet Propulsion Laboratory (JPL) of the National Aeronautics and Space Administration (NASA) for their decisive contributions to the success of SWICS and the Ulysses mission. We are indebted to P. Bochsler and M. C. E. Huber for valuable discussions. This work was supported by the Swiss National Science Foundation, NASA-JPL contract 955460, and the Minister für Forschung und Technologie of Germany.

31 January 1995; accepted 20 April 1995

Requirement of a Small Cytoplasmic RNA for the Establishment of Thermotolerance

Peter A. Fung, Jacek Gaertig, Martin A. Gorovsky, Richard L. Hallberg*

Thermotolerance is an inducible state that endows cells with an enhanced resistance to thermal killing. Heat shock proteins are believed, and in a few instances have been shown, to be the agents conferring this resistance. The role of a small cytoplasmic RNA (G8 RNA) in developing thermotolerance in *Tetrahymena thermophila* was investigated by creating a strain devoid of all functional G8 genes. These G8 null cells mounted an apparently normal heat shock response, but they were unable to establish thermotolerance.

A strong positive correlation between the accumulation of heat shock proteins (hsps) and the ability of cells to maintain viability at or above normally lethal temperatures has been noted for a number of years (*1*). However, recently it has been shown that specific stress-induced proteins are absolutely required for the establishment of thermotolerance (*2*).

We previously showed that, in response to heat shock, starvation, or entry into the stationary growth phase, the ciliated protozoan *Tetrahymena thermophila* rapidly accumulates a small cytoplasmic RNA (approximately 300 nucleotides) called G8 that quantitatively associates with ribosomes (*3*–*5*). Unlike other heat-inducible genes, the gene encoding G8 RNA is transcribed by RNA polymerase III (*3*). The kinetics of accumulation of G8 RNA on ribosomes coincides with changes in the fractions of hsp and non-hsp mRNAs translated during heat shock (*3*, *6*, *7*). G8 RNA shares weak homology with 7SL and 4.5S RNA (*4*), two RNAs known to affect ribosome function (*8*). Furthermore, as revealed by Northern (RNA) blot analysis, G8 RNA forms a stable duplex with the large (28S) but not the small (18S) ribosomal RNA; antisense G8 RNA hybridizes to neither (*9*). We therefore proposed that G8 RNA might be part of a machinery that regulates selective translation of different classes of mRNA during stress situations (*4*).

To test this hypothesis, we used genetic manipulation methods (*10*–*12*) to create a strain of *T. thermophila* in which the approximately 50 macronuclear copies of the gene encoding G8 RNA were inactivated by insertion of a neomycin (*neo*) gene (Fig. 1A) (*13*). Expression of the *neo* gene confers on *T. thermophila* an increased resistance to paromomycin (*12*). Although initial transformants contained copies of both the functional and the inactivated G8 gene, the continued growth of such cells in increasingly higher concentrations of paromomycin eventually selected for cells that contained only the disrupted form of the gene (Fig. 1B). G8 null cells did not produce G8 RNA when starved or when exposed to a 39°C heat shock for 2 hours (Fig. 1, C and D), conditions that normally enhance expression of G8 RNA (*3*, *4*). These results indicated that the G8 gene is not essential for normal vegetative growth.

To investigate whether G8 RNA is required during heat shock, we transferred early logarithmic phase wild-type and G8 null cells from 30°C to 39°C and maintained them at 39°C for 24 hours. Under these conditions, wild-type cells initially stop growing and synthesize predominantly hsps for about 1.5 hours (*7*, *14*, *15*). As the synthesis of non-hsps returns, growth recommences, albeit at a reduced rate (*14*). The synthesis of hsps and the return to non-hsp synthesis in G8 null cells appeared almost normal, although the return of non-

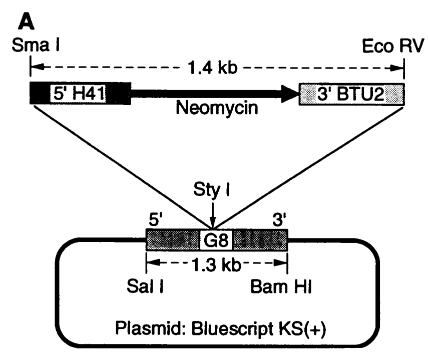

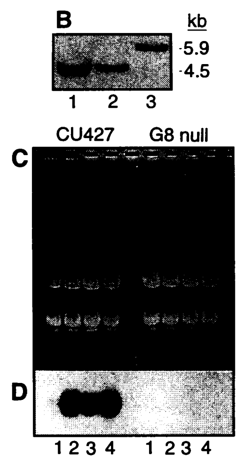

Fig. 1. Generation of a G8 deletion strain. (**A**) Construction of a G8 gene disrupted with a neomycin gene (*13*). (**B**) Southern (DNA) blot analysis of strains with and without disrupted copies of the G8 gene. DNA was cut with Eco RI, subjected to electrophoresis on a 0.8% agarose gel, transferred to a filter, and probed with a ^{32}P-labeled antisense copy of the G8 gene generated by in vitro transcription of a linearized Bluescript plasmid (pBS) containing a complementary DNA copy of G8 RNA (*3*). The sizes of the labeled fragments were determined by comparison with Hind III–cut λ DNA. Lane 1, wild type (CU427); lane 2, BTU2 null; and lane 3, G8 null. (**C** and **D**) Northern blot analysis of G8 RNA isolated from CU427 or G8 null cells. Total RNA was isolated as in (*4*). Lanes 1, cells in early log phase at 30°C; lanes 2, cells shifted to 39°C for 2 hours; lanes 3, cells transferred to starvation medium for 2 hours; and lanes 4, cells in starvation medium for 5 hours. The gels were stained with ethidium bromide (C), and the RNA was then transferred to a filter that was hybridized to a ^{32}P-labeled antisense copy of G8 RNA and autoradiographed (D).

P. A. Fung and R. L. Hallberg, Department of Biology, Syracuse University, Syracuse, NY 13244, USA.
J. Gaertig and M. A. Gorovsky, Department of Biology, University of Rochester, Rochester, NY 14627, USA.

*To whom correspondence should be addressed.